

Thermodynamics of ideal quantum gas with fractional statistics in \mathcal{D} dimensions

Geoffrey G. Potter,¹ Gerhard Müller,¹ and Michael Karbach^{2,1}

¹ *Department of Physics, University of Rhode Island, Kingston RI 02881, USA*

² *Bergische Universität Wuppertal, Fachbereich Mathematik und Naturwissenschaften, D-42097 Wuppertal, Germany*

(Dated: July 3, 2018)

We present exact and explicit results for the thermodynamic properties (isochores, isotherms, isobars, response functions, velocity of sound) of a quantum gas in dimensions $\mathcal{D} \geq 1$ and with fractional exclusion statistics $0 \leq g \leq 1$ connecting bosons ($g = 0$) and fermions ($g = 1$). In $\mathcal{D} = 1$ the results are equivalent to those of the Calogero-Sutherland model. Emphasis is given to the crossover between boson-like and fermion-like features, caused by aspects of the statistical interaction that mimic long-range attraction and short-range repulsion. The full isochoric heat capacity and the leading low- T term of the isobaric expansivity in $\mathcal{D} = 2$ are independent of g . The onset of Bose-Einstein condensation along the isobar occurs at a nonzero transition temperature in all dimensions. The T -dependence of the velocity of sound is in simple relation to isochores and isobars. The effects of soft container walls are accounted for rigorously for the case of a pure power-law potential.

I. INTRODUCTION

A whole new arena for the study of effects of dimensionality has opened up in the wake of the advances in instrumentation achieved in the research that led to the observation of Bose-Einstein condensates [1, 2]. The magnetic and optical traps that were developed and perfected in this and related lines of research can also be made in shapes that effectively constrain the kinematics of trapped gas atoms to fewer than $\mathcal{D} = 3$ dimensions [3, 4, 5, 6].

In cigar-shaped traps, for example, the energy states of single particles with nonzero momentum components perpendicular to the axis are frozen out for the most part at low enough temperature. In disk-shaped traps the only energy states with significant occupancy at low T are those with zero momentum component perpendicular to the plane. We are then dealing, effectively, with quantum gases in dimensions $\mathcal{D} = 1$ and $\mathcal{D} = 2$, respectively. A further effective change in spatial dimensionality can be produced by controlling the firmness of the trap walls [7, 8].

Of no less importance than effects of dimensionality are, of course, effects of interaction. They are notoriously difficult to handle in any effort that goes beyond mean-field theory or low-order perturbation calculations. Here a little explored non-perturbative approach presents itself as a promising alternative: the thermodynamic analysis of statistically interacting quantum gases. Statistical interaction grew out of the concept of fractional exclusion statistics, introduced as a tool to interpret the quasiparticle composition of the eigenstates in exactly solvable quantum many-body systems [9].

The thermodynamics of statistically interacting degrees of freedom is amenable to exact analysis under very general circumstances [10]. A most remarkable link exists between the *dynamical* interaction in the form of a coupling term in the many-body Hamiltonian and the *statistical* interaction in the form of a generalized Pauli principle. For certain solvable models in $\mathcal{D} = 1$ one can

replace the former by the latter and arrive at equivalent thermodynamic properties [11].

The chances for extending any known exact solution for a dynamically interacting quantum gas to $\mathcal{D} > 1$ are slim because the criteria for purely nondiffractive scattering [12] are unlikely to be satisfied apart from highly contrived scenarios. By contrast, extending the exact solution for a statistically interacting quantum gas to higher dimensions is straightforward conceptually if not technically.

Notwithstanding the absence of an exact correspondence between dynamical and statistical interactions in $\mathcal{D} > 1$, the exact thermodynamics of statistically interacting degrees of freedom has the potential of displaying a richness in phenomena unrivaled by mean-field theory or by perturbative approaches. Most importantly, it incorporates a full and consistent account of fluctuations.

Here we consider a statistical interaction limited to particles with identical momenta, in which case it reduces to a statistical exclusion condition. The two parameters of the system explored here are the coefficient of exclusion statistics, $0 \leq g \leq 1$, which spans a bridge between bosons ($g = 0$) and fermions ($g = 1$), and the dimensionality $\mathcal{D} \geq 1$. While this system does exhibit the attributes typical for an ideal quantum gas, several of the highlighted features are indicative of specific aspects of the statistical interaction including features of long-range attraction and short-range repulsion. Selected results are known from previous work [13, 14, 15, 16].

A brief review of fractional exclusion statistics and its use in statistical mechanics is found in Sec. II. The application of these statistical mechanical tools to the model system under consideration is described in Sec. III. The exact thermodynamics of the ideal quantum gas with fractional exclusion statistics in a \mathcal{D} -dimensional box with rigid walls is presented in Sec. IV. The impact of soft container walls as might be relevant in the context of atomic traps is discussed in Sec. V. The main results are assessed in Sec. VI as benchmarks for corresponding results pertaining to quantum gases with less constrained

statistical interactions as are forthcoming from work in progress [17].

II. FRACTIONAL EXCLUSION STATISTICS

The core relation of exclusion statistics is a generalized Pauli principle as introduced by Haldane [9]. It expresses how the number of states available to one particle is affected by the presence of other particles:

$$\Delta d_i = -g_i \Delta n_i, \quad (1)$$

where the index i enumerates distinct particle species (a flexible notion) and the g_i are coefficients of (fractional) exclusion statistics. For free bosons we have $g_i = 0$ and for free fermions $g_i = 1$. Integrating Eq. (1) yields the dimensionality of the *one-particle* Hilbert space in the presence of n_i particles of species i :

$$d_i = A_i - g_i(n_i - 1), \quad (2)$$

where A_i are constants. The dimensionality of the *many-particle* Hilbert space is

$$W = \prod_i \binom{d_i + n_i - 1}{n_i}, \quad (3)$$

where each factor represents the simple combinatorial problem of placing n_i particles among $d_i + n_i - 1$ distinct states available to them.

A system of (dynamically) free quasiparticles with fractional exclusion statistics has two principal specifications: (i) a set of orbitals at energies ϵ_i and (ii) a set of statistical exclusion coefficients g_i . The grand partition function is of the form [10, 18]

$$Z = \prod_i \left[\frac{1 + w_i}{w_i} \right], \quad (4)$$

where the w_i are determined by the nonlinear algebraic equations

$$\frac{\epsilon_i - \mu}{k_B T} = \ln(1 + w_i) - g_i \ln \left(\frac{1 + w_i}{w_i} \right). \quad (5)$$

The energy level occupancies $\langle n_i \rangle$ are inferred from the w_i as

$$\langle n_i \rangle = \frac{1}{w_i + g_i}. \quad (6)$$

To illustrate the link between the combinatorial expression (3) and the statistical mechanical expression (4) we consider an open system of M orbitals populated by (dynamically) free particles with (uniform) exclusion coefficients $g > 0$. The number of distinct n -particle configurations implied by (3) is

$$\begin{aligned} W_n(M) &= \binom{A + (1 - g)(n - 1)}{n} \\ &= \frac{\Gamma(A + n - g(n - 1))}{\Gamma(n + 1)\Gamma(A - g(n - 1))}, \end{aligned} \quad (7)$$

where A is to be adjusted so as to yield integer values for $W_n(M)$ and a meaningful maximum capacity n_{\max} . For integer g we use $A = M$. For $g = \frac{1}{2}$ we use $A = M$ if M is odd and $A = M + \frac{1}{2}$ if M is even. This scheme is naturally extended to other fractional values of g , limiting the maximum capacity to $n_{\max} < (M + g)/g$.

The dimensionality of the Fock space,

$$W_{\text{tot}}(M) = \sum_{n=0}^{n_{\max}} W_n(M), \quad (8)$$

can be expressed, for integer g , as a (higher-order) Lamé sequence,

$$W_{\text{tot}}(M) = M + 1 \quad (9)$$

for $M = 0, 1, \dots, g - 1$ and

$$W_{\text{tot}}(M) = W_{\text{tot}}(M - 1) + W_{\text{tot}}(M - g) \quad (10)$$

for $M = g, g + 1, \dots$. In the case of fermions ($g = 1$) we obtain $W_{\text{tot}}(M) = 2^M$ and for $g = 2$ a string of Fibonacci numbers: $W_{\text{tot}}(M) = F_M = 1, 2, 3, 5, 8, \dots$. For semions ($g = \frac{1}{2}$) we use (7). The result is a string of alternate Fibonacci numbers: $W_{\text{tot}}(M) = F_{2M+1} = 1, 3, 8, \dots$.

The quantity we investigate for our illustration is the limit $M \rightarrow \infty$ of the proportion by which the number of many-particle states increases if we add one orbital to the system: $R_M \doteq W_{\text{tot}}(M + 1)/W_{\text{tot}}(M)$. For fermions we have $R_M = 2$ independent of M as expected. For semions we obtain the square of the golden section:

$$R_M = \frac{F_{2M+3}}{F_{2M+1}} \xrightarrow{M \rightarrow \infty} \left[\frac{1}{2} (\sqrt{5} + 1) \right]^2. \quad (11)$$

Now we derive R_∞ directly from (4) and (5) at $T = \infty$:

$$R_\infty = \frac{1 + w}{w}, \quad w^g (1 + w)^{1-g} = 1. \quad (12)$$

The solution for fermions is $w = 1$, yielding $R_\infty = 2$ as before via combinatorics. In the semion case the asymptotic result in (11) is recovered from the solution of the quadratic equation in (12).

III. QUANTUM GAS WITH FRACTIONAL STATISTICS

Before we go on to discuss how Eqs. (4)–(6) are applied to a quantum gas in \mathcal{D} dimensions, we turn to an exactly solved model in $\mathcal{D} = 1$.

A. Calogero-Sutherland model

The Calogero-Sutherland (CS) model describes massive particles on a ring of circumference L with a (dynamical) pair interaction (in units where $\hbar^2/2m = 1$)

[13, 19, 20, 21]:

$$H = - \sum_{i=1}^N \frac{\partial^2}{\partial x_i^2} + \sum_{j < i} \frac{2g(g-1)}{d_{ij}^2}. \quad (13)$$

Here

$$d_{ij} = \left| \frac{L}{\pi} \sin \left(\frac{\pi}{L} (x_i - x_j) \right) \right| \quad (14)$$

represents the chord distance on the ring between particles. Varying the parameter g across the interval $0 \leq g \leq 1$, amounts to a parametric link between free bosons ($g = 0$) and free fermions ($g = 1$).

The spectrum and thermodynamics of the CS model can be described by an asymptotic coordinate Bethe ansatz [12]. The thermodynamic Bethe ansatz inferred therefrom expresses the grand potential in the form

$$\Omega(T, L, \mu) = -k_B T \left(\frac{L}{2\pi} \right) \int_{-\infty}^{+\infty} dk \ln \left(1 + e^{-\epsilon(k)/k_B T} \right), \quad (15)$$

where $\epsilon(k)$ is determined by the Yang-Yang-type equation [22]

$$\begin{aligned} \epsilon(k) &= k^2 - \mu \\ &- \frac{k_B T}{2\pi} \int_{-\infty}^{+\infty} dk' K(k - k') \ln \left(1 + e^{-\epsilon(k')/k_B T} \right) \end{aligned} \quad (16)$$

with kernel

$$K(k - k') = 2\pi(1 - g)\delta(k - k'). \quad (17)$$

The distribution of particles, $\rho_P(k)$, is found to be the solution, for given $\epsilon(k)$, of the Lieb-Liniger-type equation [23]

$$2\pi\rho_P(k) \left[1 + e^{\epsilon(k)/k_B T} \right] = 1 + \int_{-\infty}^{+\infty} dk' K(k - k')\rho_P(k'). \quad (18)$$

B. Generalization of CS model

Returning to statistical interaction we consider a non-relativistic gas in a rigid box of dimensionality \mathcal{D} and volume $V = L^{\mathcal{D}}$ with energy-momentum relation $\epsilon_0(k) = |\mathbf{k}^2|$ and exclusion statistics

$$g(\mathbf{k} - \mathbf{k}') = g\delta(\mathbf{k} - \mathbf{k}'). \quad (19)$$

The grand potential derived from (4) becomes

$$\Omega = -k_B T \left(\frac{L}{2\pi} \right)^{\mathcal{D}} \int d^{\mathcal{D}}k \ln \frac{1 + w_{\mathbf{k}}}{w_{\mathbf{k}}}, \quad (20)$$

where $w_{\mathbf{k}}$ is the solution of

$$\frac{|\mathbf{k}|^2 - \mu}{k_B T} = \ln(1 + w_{\mathbf{k}}) - g \ln \frac{1 + w_{\mathbf{k}}}{w_{\mathbf{k}}}. \quad (21)$$

The particle density in \mathbf{k} -space is represented by the function

$$\langle n_{\mathbf{k}} \rangle = \frac{1}{w_{\mathbf{k}} + g}. \quad (22)$$

The fundamental thermodynamic relations, from which most thermodynamic properties are conveniently derived, are integrals involving $w_{\mathbf{k}}$ and $\langle n_{\mathbf{k}} \rangle$:

$$\frac{pV}{k_B T} = \left(\frac{L}{2\pi} \right)^{\mathcal{D}} \int d^{\mathcal{D}}k \ln \frac{1 + w_{\mathbf{k}}}{w_{\mathbf{k}}}, \quad (23)$$

$$\mathcal{N} = \left(\frac{L}{2\pi} \right)^{\mathcal{D}} \int d^{\mathcal{D}}k \langle n_{\mathbf{k}} \rangle, \quad (24)$$

$$U = \left(\frac{L}{2\pi} \right)^{\mathcal{D}} \int d^{\mathcal{D}}k |\mathbf{k}|^2 \langle n_{\mathbf{k}} \rangle. \quad (25)$$

These relations state the dependence of the pressure p , the average number of particles \mathcal{N} , and the internal energy U on fugacity z , temperature T , and volume V . They are also known as the *thermodynamic* equation of state (23)-(24) and the *caloric* equation of state (24)-(25).

It was recognized [11, 18, 24] that the thermodynamic Bethe ansatz solution (15)–(18) of the CS model is equivalent to the solution of a statistical interacting gas as presented above for $\mathcal{D} = 1$ if we make the following identifications:

$$w_k = \exp \left(\frac{\epsilon(k)}{k_B T} \right), \quad \langle n_k \rangle = 2\pi\rho_P(k), \quad (26)$$

$$g(k, k') = \delta(k - k') - \frac{1}{2\pi} K(k - k'). \quad (27)$$

For the thermodynamic extension to $\mathcal{D} \geq 1$ of the CS model we use the statistical interaction (19) and the density of 1-particle states of the nonrelativistic ideal gas,

$$D_0(\epsilon_0) = \left(\frac{L}{2\pi} \right)^{\mathcal{D}} \frac{\pi^{\mathcal{D}/2}}{\Gamma(\mathcal{D}/2)} \epsilon_0^{\mathcal{D}/2-1}, \quad (28)$$

to rewrite Eqs. (20)–(22) in the form

$$\Omega = -k_B T \int_0^{\infty} d\epsilon_0 D_0(\epsilon_0) \ln \frac{1 + w(\epsilon_0)}{w(\epsilon_0)}, \quad (29)$$

$$\frac{1}{z} \exp \left(\frac{\epsilon_0}{k_B T} \right) = [w(\epsilon_0)]^g [1 + w(\epsilon_0)]^{1-g}, \quad (30a)$$

$$z = \exp(\mu/k_B T), \quad (30b)$$

$$\langle n(\epsilon_0) \rangle = \frac{1}{w(\epsilon_0) + g}, \quad (31)$$

and to reduce Eqs. (23)–(25) to integrals over functions of ϵ_0 .

C. Average level occupancy

In ideal quantum gases the average level occupancy $\langle n(\epsilon_0) \rangle$ is a unique function of $(\epsilon_0 - \mu)/k_B T$ independent of \mathcal{D} . A plot of this function for the generalized CS model is shown in Fig. 1 for various values of g . In the boson case we have $w(\epsilon_0) = e^{(\epsilon_0 - \mu)/k_B T} - 1$ and in the fermion case $w(\epsilon_0) = e^{(\epsilon_0 - \mu)/k_B T}$. For semions we have

$$w(\epsilon_0) = \sqrt{[e^{(\epsilon_0 - \mu)/k_B T}]^2 + \frac{1}{4}} - \frac{1}{2}. \quad (32)$$

The exact analytic solution of (30) with $0 < g < 1$ is known in a series representation [16]. The asymptotic level occupancy for $(\epsilon_0 - \mu)/k_B T \rightarrow -\infty$ is $1/g$.

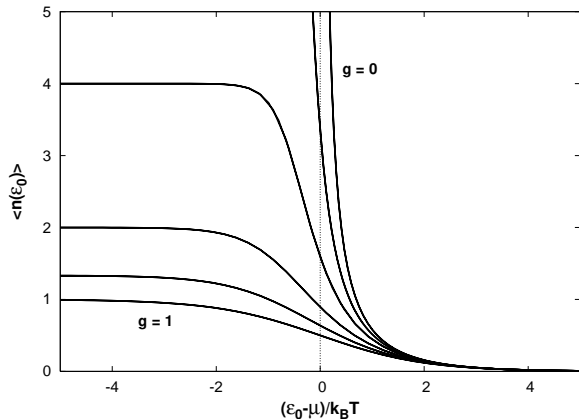


FIG. 1: Average level occupancy $\langle n(\epsilon_0) \rangle$ versus $(\epsilon_0 - \mu)/k_B T$ for $g = 0, 0.1, 0.25, 0.5, 0.75, 1$ (from top down).

IV. THERMODYNAMICS OF THE GENERALIZED CS MODEL

Exact and explicit results for the thermodynamics of the generalized CS model can now be calculated from the general expressions derived in Sec. III.

A. CS functions

Introducing the CS functions

$$G_n(z, g) \doteq \frac{1}{\Gamma(n)} \int_0^\infty dx \frac{x^{n-1}}{\bar{w}(x) + g}, \quad (33)$$

$$[\bar{w}(x)]^g [1 + \bar{w}(x)]^{1-g} = \frac{e^x}{z}, \quad (34)$$

for $n > 0$ we rewrite Eqs. (23)–(25) as

$$\frac{p\lambda_T^{\mathcal{D}}}{k_B T} = G_{\mathcal{D}/2+1}(z, g), \quad (35)$$

$$\frac{\mathcal{N}\lambda_T^{\mathcal{D}}}{V} = G_{\mathcal{D}/2}(z, g) \left[+ \frac{z}{1-z} \right], \quad (36)$$

$$\frac{U\lambda_T^{\mathcal{D}}}{V} / \left(\frac{\mathcal{D}}{2} k_B T \right) = G_{\mathcal{D}/2+1}(z, g), \quad (37)$$

where

$$\lambda_T \doteq \sqrt{\frac{h^2}{2\pi m k_B T}} \xrightarrow{h^2/2m=1} \sqrt{\frac{4\pi}{k_B T}} \quad (38)$$

is the thermal wavelength and the term in (36) enclosed by brackets is relevant only if $g = 0$ and $\mathcal{D} > 2$. For $g = 0$ and $g = 1$ the CS functions become the Bose-Einstein (BE) functions and Fermi-Dirac (FD) functions, respectively. The range of fugacity is $0 \leq z \leq 1$ for bosons. For all other cases z has no upper bound.

The overall shape of the CS functions is illustrated in Fig. 2. For $\frac{1}{2} \leq g \leq 1$ the curves are concave. For $0 < g \leq \frac{1}{2}$ they have a convex portion at small z and then switch to concave behavior. The curve for $g = 0$ is convex over its entire (restricted) domain.

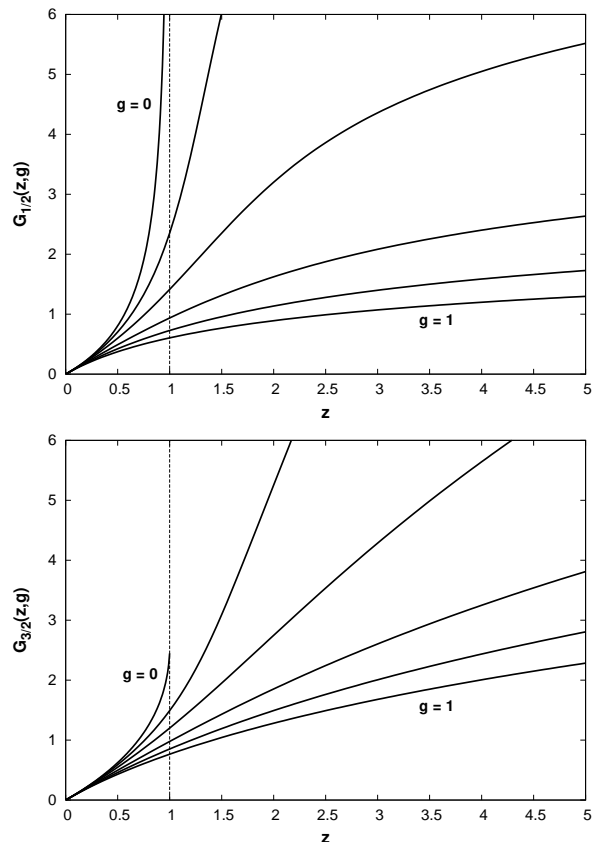


FIG. 2: CS functions (33) for $n = \frac{1}{2}, \frac{3}{2}$ plotted versus z for $g = 0, 0.1, 0.25, 0.5, 0.75$ (from top down).

The CS functions have the following power series expansions [16]:

$$\begin{aligned} G_n(z, g) &= \sum_{l=1}^{\infty} \frac{z^l}{l^n} \frac{\Gamma(l - lg)}{\Gamma(l)\Gamma(1 - lg)} \\ &= z + \frac{z^2}{2^n}(1-2g) + \frac{z^3}{3^n}(1-3g) \left(1 - \frac{3}{2}g\right) + \mathcal{O}(z^4). \end{aligned} \quad (39)$$

The radius of convergence depends on g :

$$r(g) = \frac{1}{g^g(1-g)^{1-g}}. \quad (40)$$

The first two terms of the asymptotic expansion for large z at $g > 0$ are [15, 16]

$$G_n(z, g) \underset{z \rightarrow \infty}{\sim} \frac{(\ln z)^n}{g\Gamma(n+1)} \left[1 + \frac{\pi^2}{6} \frac{gn(n-1)}{(\ln z)^2} + \dots \right]. \quad (41)$$

The familiar recurrence relation for FD and BE functions is valid for the CS functions in general:

$$z \frac{\partial}{\partial z} G_{n+1}(z, g) = G_n(z, g). \quad (42)$$

We also use (42) to extend the definition (33) to $n \leq 0$.

B. Equation of state

The functional relationship between $pV/\mathcal{N}k_B T$ and fugacity z ,

$$\frac{pV}{\mathcal{N}k_B T} = \frac{G_{\mathcal{D}/2+1}(z, g)}{G_{\mathcal{D}/2}(z, g)}, \quad (43)$$

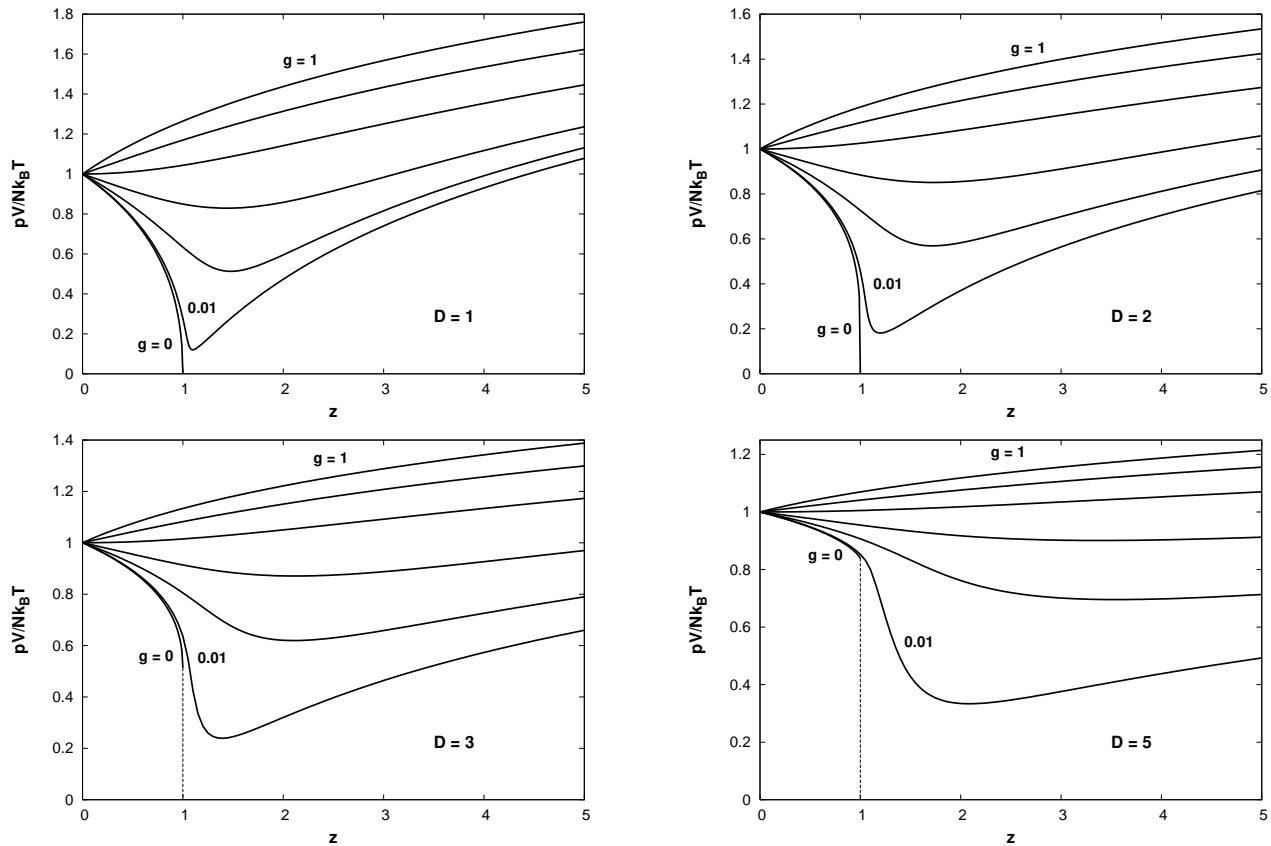


FIG. 3: Equation of state (43) in $\mathcal{D} = 1, 2, 3, 5$ for $g = 0, 0.01, 0.1, 0.25, 0.5, 0.75, 1$ (from bottom up). Note the different vertical scales.

as inferred from (35) and (36), highlights the deviations from Maxwell-Boltzmann (MB) behavior. Numerical re-

sults of $pV/\mathcal{N}k_B T$ versus z are presented in Fig. 3. In-

creasing z means, for example, decreasing T at fixed \mathcal{N}/V or increasing \mathcal{N}/V at fixed T . Any downward (upward) deviation from $pV/\mathcal{N}k_B T = 1$ is suggestive of a boson-like (fermion-like) feature.

The curves for $g > \frac{1}{2}$ exhibit a fermion-like monotonic increase over the entire range of z . The curves for $0 < g < \frac{1}{2}$ start out with (boson-like) negative slope. They reach a smooth minimum and then grow without bound in fermion-like manner. The case $g = 0$ is exceptional. Here the curve ends in a cusp singularity at $z = 1$. In $\mathcal{D} = 1$ and $\mathcal{D} = 2$ the pressure is zero at the singularity. The endpoint of the curve occurs at $T = 0$ or $\mathcal{N}/V = \infty$. In $\mathcal{D} > 2$ the pressure is nonzero at the singularity, and the endpoint of the curve signals the onset of a Bose-Einstein condensate (BEC). For fixed \mathcal{N}/V this happens at $T > 0$. The condensation proceeds along the dashed line.

The physics underlying the crossover between boson-like and fermion-like behavior may be interpreted by attributing to the statistical interaction of the generalized CS model a long-range attractive part and a shorter-range repulsive part. The repulsive core is present for all $g > 0$. The attractive part is only perceptible for $g < \frac{1}{2}$. The former prevents the collapse of the system into a BEC at $g > 0$. The latter causes a negative interaction pressure for $g < \frac{1}{2}$ (a reduction of p relative to the kinetic pressure of the MB gas) if the average interparticle distance in units of the thermal wavelength is sufficiently large.

The interplay between the two parts of the statistical interaction upon variation of the parameters g and \mathcal{D} produces a host of interesting thermodynamic effects. Their appearance in isochores, isotherms, isobars, response functions, and in the velocity of sound will be discussed in the following. For this purpose we introduce reference values for temperature T , reduced volume $v \doteq V/\mathcal{N}$, and pressure p , based on the equation of state, $p v = k_B T$ of the MB gas and the criterion that the average reference volume per particle is a hypercubic box with sides equal to the thermal wavelength (38). For isochoric, isothermal, and isobaric processes we thus use

$$\begin{aligned} k_B T_v &= \frac{4\pi}{v^{2/\mathcal{D}}}, & p_v &= \frac{4\pi}{v^{2/\mathcal{D}+1}} & (v = \text{const.}) \\ v_T &= \left(\frac{4\pi}{k_B T}\right)^{\mathcal{D}/2}, & p_T &= \frac{(k_B T)^{\mathcal{D}/2+1}}{(4\pi)^{\mathcal{D}/2}} & (T = \text{const.}) \\ k_B T_p &= (4\pi)^{\frac{\mathcal{D}}{\mathcal{D}+2}} p^{\frac{2}{\mathcal{D}+2}}, & v_p &= (4\pi/p)^{\frac{\mathcal{D}}{\mathcal{D}+2}} & (p = \text{const.}) \end{aligned}$$

These reference values are well-behaved in the boson limit, which is an advantage for our comparative plots. For some purposes (limited to $g > 0$) an alternative choice, based on the chemical potential at $T = 0$, will be more convenient.

C. Isochores

The dependence of p on T at constant v can be extracted from (35) and (36):

$$\frac{p}{p_v} = \frac{G_{\mathcal{D}/2+1}(z, g)}{[G_{\mathcal{D}/2}(z, g)]^{1+2/\mathcal{D}}}, \quad (44a)$$

$$\frac{T}{T_v} = \frac{1}{[G_{\mathcal{D}/2}(z, g)]^{2/\mathcal{D}}} \quad (44b)$$

with no restriction on z for $0 < g \leq 1$. In Fig. 4 we show isochores for various g and \mathcal{D} . Each curve represents a universal isochore, valid for arbitrary values of v . The shape of the curves at high T reflects the emerging MB behavior. The leading correction term in the high- T expansion of (44),

$$\frac{p}{p_v} \stackrel{T \rightarrow \infty}{\rightsquigarrow} \frac{T}{T_v} \left[1 - \frac{1/2 - g}{2^{\mathcal{D}/2}} \left(\frac{T_v}{T}\right)^{\mathcal{D}/2} \right], \quad (45)$$

describes bundles of isochores whose vertical separations increase with increasing T/T_v if $\mathcal{D} < 2$, stay constant if $\mathcal{D} = 2$, and decrease if $\mathcal{D} > 2$. The deviation from the MB isochore, $p/p_v = T/T_v$, is negative for $g < \frac{1}{2}$ and positive for $g > \frac{1}{2}$, decreasing in magnitude as \mathcal{D} increases. For semions the deviation is of higher order in T_v/T .

The intercept of the isochore at $T = 0$ as extracted from the leading term in the asymptotic expansion of (44) is

$$\frac{p_0}{p_v} = \frac{\bar{T}_v}{T_v} \frac{1}{\mathcal{D}/2 + 1}, \quad (46a)$$

$$\frac{\bar{T}_v}{T_v} = [g\Gamma(\mathcal{D}/2 + 1)]^{2/\mathcal{D}}, \quad (46b)$$

where $\mu_0 = k_B \bar{T}_v$ is the chemical potential at $T = 0$. If we replot the data for $g > 0$ in Fig. 4 as p/\bar{p}_v versus T/\bar{T}_v with $\bar{p}_v = p_v(T/\bar{T}_v)$ we obtain the MB isochore in the limit $\mathcal{D} \rightarrow \infty$.

In the boson case, Eq. (44) is still valid for $z < 1$. This covers the full T -range in $\mathcal{D} \leq 2$. In $\mathcal{D} > 2$ in the limit $z \rightarrow 1$ occurs at

$$\frac{p_c}{p_v} = \frac{\zeta(\mathcal{D}/2 + 1)}{[\zeta(\mathcal{D}/2)]^{2/\mathcal{D}+1}}, \quad (47a)$$

$$\frac{T_c}{T_v} = \frac{1}{[\zeta(\mathcal{D}/2)]^{2/\mathcal{D}}}, \quad (47b)$$

where $G_n(1, 0) = \zeta(n)$ is the Riemann zeta function. The values p_c, T_c mark the onset of a BEC. Note that T_c begins to rise from zero at $\mathcal{D} = 2$ and approaches the value T_v as $\mathcal{D} \rightarrow \infty$. The bosonic isochore in the coexistence region is

$$\frac{p}{p_v} = \left(\frac{T}{T_v}\right)^{\mathcal{D}/2+1} \zeta(\mathcal{D}/2 + 1) \quad (T < T_c). \quad (48)$$

The singularity at $T_c > 0$ becomes stronger as \mathcal{D} increases. For $2 < \mathcal{D} \leq 4$, there is a discontinuity in curva-

ture. It turns into a discontinuity in slope for $\mathcal{D} > 4$ and becomes a discontinuity in the function itself for $\mathcal{D} = \infty$.

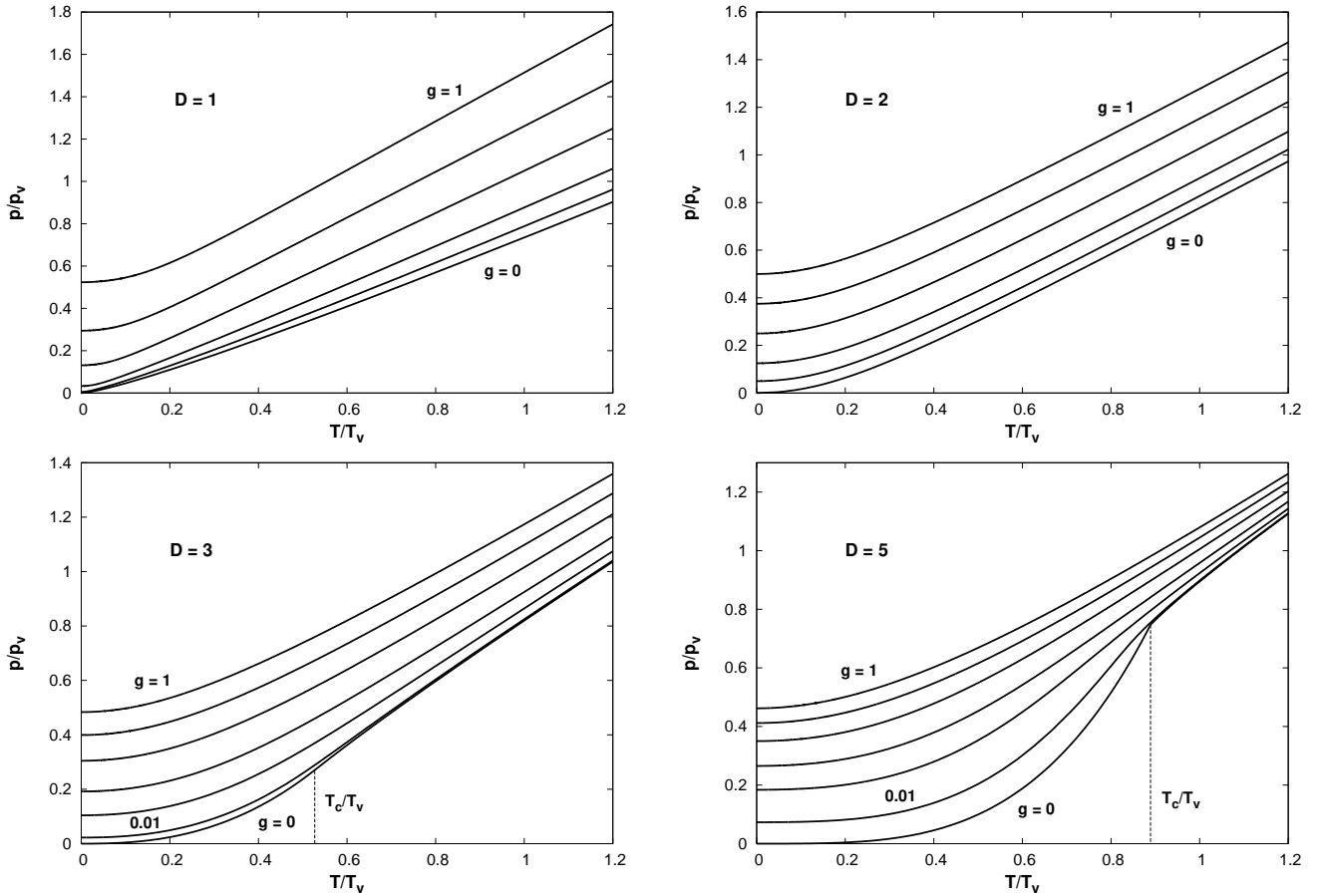


FIG. 4: Isochores in $\mathcal{D} = 1, 2, 3, 5$ for $g = 0, 0.01, 0.1, 0.25, 0.5, 0.75, 1$ (from bottom up). In $\mathcal{D} = 1, 2$ the curves for $g = 0, 0.01$ are unresolved. Note the different vertical scales.

D. Isotherms

The dependence of p on v at constant T in a parametric representation follows again from (35) and (36):

$$\frac{p}{p_T} = G_{\mathcal{D}/2+1}(z, g), \quad (49a)$$

$$\frac{v}{v_T} = \frac{1}{G_{\mathcal{D}/2}(z, g)} \quad (49b)$$

applicable for $0 < g \leq 1$ with unrestricted z and for $g = 0$ with $z \leq 1$. In Fig. 5 we show isotherms for various g and \mathcal{D} . The convergence of the curves in the low-density regime reflects the emerging MB behavior. The leading correction to Boyle's law,

$$\frac{p}{p_T} \xrightarrow{v \rightarrow \infty} \frac{v_T}{v} \left[1 - \frac{1/2 - g}{2^{\mathcal{D}/2}} \left(\frac{v_T}{v} \right) \right], \quad (50)$$

is negative for $g < \frac{1}{2}$ and positive for $g > \frac{1}{2}$. It weakens in magnitude as \mathcal{D} increases. The divergence of the isochores for $g > 0$ in the high-density limit is of the form

$$\left(\frac{p}{p_T} \right) \left(\frac{v}{v_T} \right)^{(\mathcal{D}+2)/\mathcal{D}} = g^{2/\mathcal{D}} \frac{[\Gamma(\mathcal{D}/2 + 1)]^{2/\mathcal{D}}}{\mathcal{D}/2 + 1}, \quad (51)$$

consistent with MB behavior for $g > 0$ in the limit $\mathcal{D} \rightarrow \infty$, if we switch to alternative reference values based on the chemical potential.

For bosons the pressure p/p_T remains finite as $v/v_T \rightarrow 0$. In $\mathcal{D} \leq 2$ the limit $z \rightarrow 1$ implies

$$\frac{v}{v_T} \rightarrow 0, \quad \frac{p}{p_T} \rightarrow \zeta \left(\frac{\mathcal{D}}{2} + 1 \right), \quad (52)$$

whereas in $\mathcal{D} > 2$ at $z = 1$ we have

$$\frac{v_c}{v_T} = \frac{1}{\zeta(\mathcal{D}/2)}, \quad \frac{p_c}{p_T} = \zeta(\mathcal{D}/2 + 1). \quad (53)$$

The intercept of the bosonic isotherm decreases with increasing \mathcal{D} and approaches unity for $\mathcal{D} \rightarrow \infty$. In $\mathcal{D} \leq 2$

the bosonic isotherm is a smooth curve. Its slope at $v/v_T = 0$ is negative in $\mathcal{D} < 2$ and zero in $\mathcal{D} = 2$. In $\mathcal{D} > 2$ the pressure is constant at p_c for $0 \leq v \leq v_c$ along the isotherm. In the limit $\mathcal{D} \rightarrow \infty$ we have the MB isotherm, $p/p_T = v_T/v$ at $v > v_T$ joined by a the constant $p/p_T = 1$ at $v/v_T < 1$.

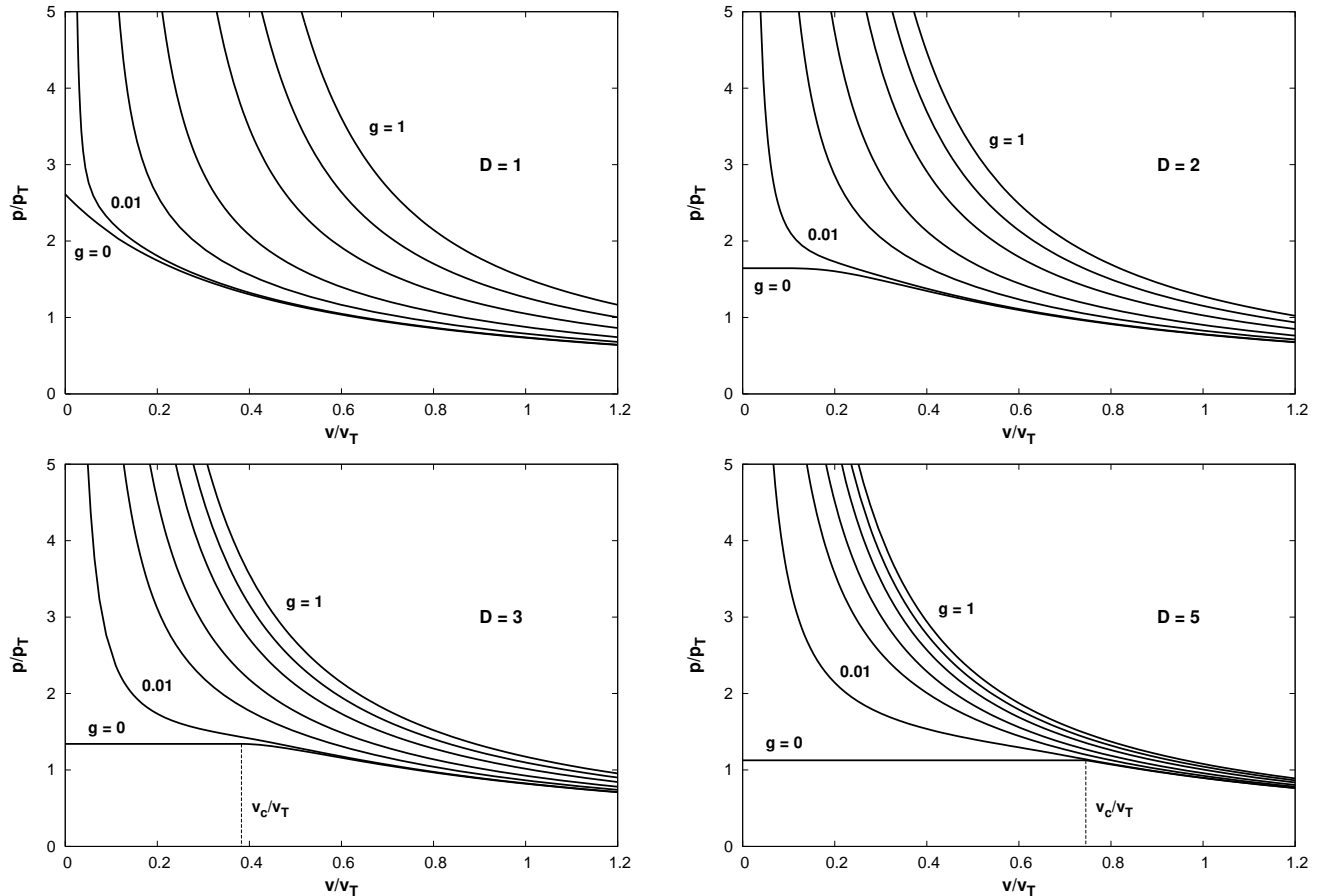


FIG. 5: Isotherms of the generalized CS model in dimensions $\mathcal{D} = 1, 2, 3, 5$ for $g = 0, 0.01, 0.1, 0.25, 0.5, 0.75, 1$ (from bottom up).

E. Isobars

The dependence of v on T at constant p is to be calculated from

$$\frac{v}{v_p} = \frac{[G_{\mathcal{D}/2+1}(z, g)]^{\mathcal{D}/(\mathcal{D}+2)}}{G_{\mathcal{D}/2}(z, g)}, \quad (54a)$$

$$\frac{T}{T_p} = \frac{1}{[G_{\mathcal{D}/2+1}(z, g)]^{2/(\mathcal{D}+2)}}, \quad (54b)$$

applicable for $0 < g \leq 1$ with unrestricted z and for $g = 0$ with $z \leq 1$. In Fig. 6 we show isobars for various g and

\mathcal{D} . The leading correction to MB behavior at high T ,

$$\frac{v}{v_p} \stackrel{T \rightarrow \infty}{\sim} \frac{T}{T_p} \left[1 - \frac{1/2 - g}{2^{\mathcal{D}/2}} \left(\frac{T_p}{T} \right)^{\mathcal{D}/2+1} \right], \quad (55)$$

explains the observation that the vertical separations of the curves in Fig. 6 decrease with increasing T/T_p in all \mathcal{D} . Again the deviation from MB behavior switches sign at $g = \frac{1}{2}$. The intercept at $T = 0$ of the isobars for $g > 0$ is

$$\lim_{T \rightarrow 0} \frac{v}{v_p} = g^{2/(\mathcal{D}+2)} \frac{[\Gamma(\mathcal{D}/2 + 1)]^{2/(\mathcal{D}+2)}}{(\mathcal{D}/2 + 1)^{\mathcal{D}/(\mathcal{D}+2)}}, \quad (56)$$

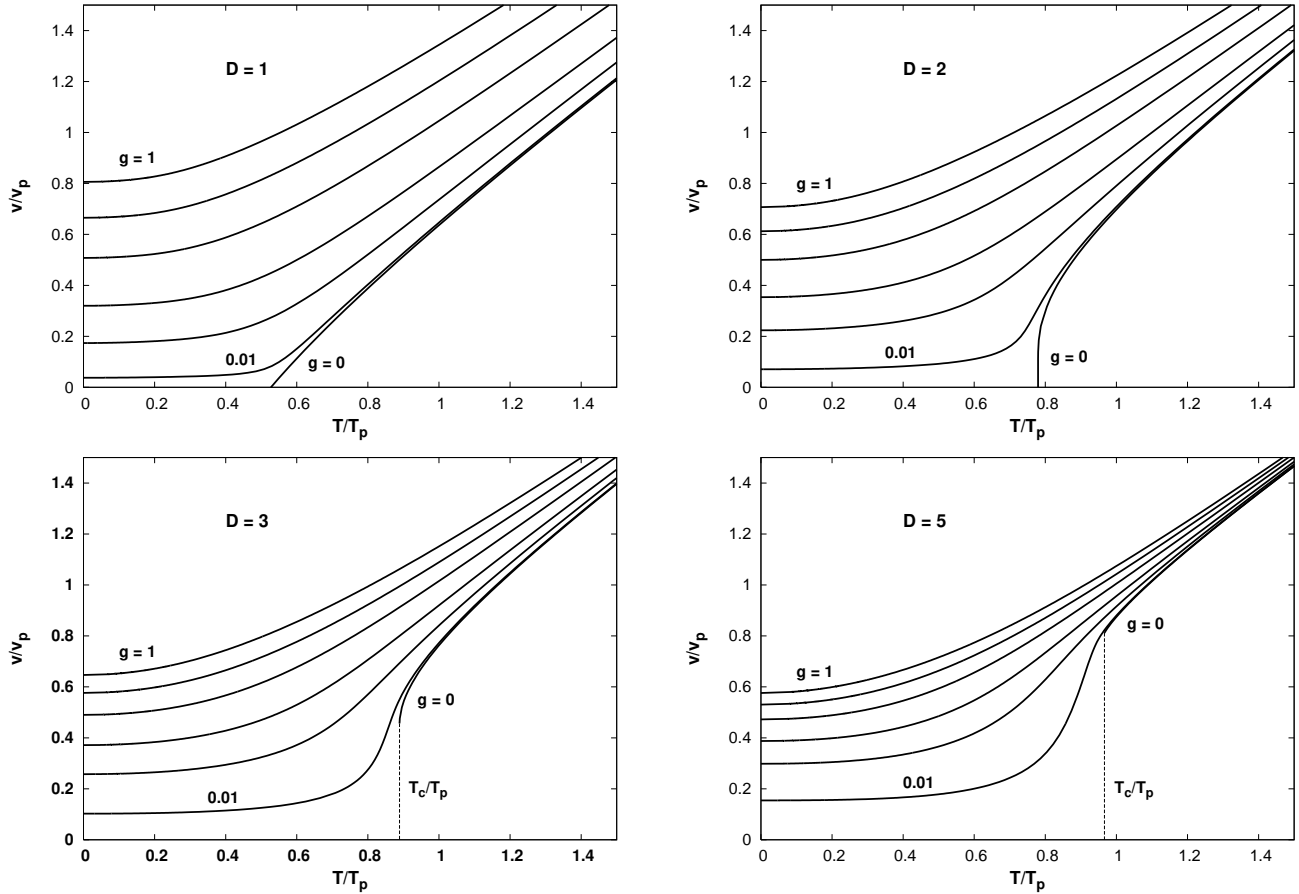


FIG. 6: Isobars in $\mathcal{D} = 1, 2, 3, 5$ for $g = 0, 0.01, 0.1, 0.25, 0.5, 0.75, 1$ (from bottom up).

again consistent with MB behavior for $g > 0$ in the limit $\mathcal{D} \rightarrow \infty$ provided we use alternative reference values based on the chemical potential.

The isobaric curves for bosons end in a critical point at

$$\frac{v_c}{v_p} = \frac{[\zeta(\mathcal{D}/2 + 1)]^{\mathcal{D}/(\mathcal{D}+2)}}{\zeta(\mathcal{D}/2)}, \quad (57a)$$

$$\frac{T_c}{T_p} = \frac{1}{[\zeta(\mathcal{D}/2 + 1)]^{2/(\mathcal{D}+2)}}. \quad (57b)$$

Note that the critical (reduced) volume is nonzero only

in $\mathcal{D} > 2$ whereas the critical temperature is nonzero in all $\mathcal{D} \geq 1$. At $T < T_c$ the boson gas is unable to maintain the prescribed pressure. In $\mathcal{D} \leq 2$ the bosonic isobar terminates in a cusp at $v/v_p = 0$. The switch from a pure gas at $T > T_c$ to a pure BEC at $T < T_c$ occurs when $v/v_p = 0$. There is no coexistence region. In $\mathcal{D} > 2$ the bosonic isobar terminates in a cusp at $T = T_c > 0$ and $v = v_c > 0$. Here the two phases do coexist. During condensation v/v_p gradually goes to zero along the vertical dashed line. With increasing \mathcal{D} both v_c/v_p and T_c/T_p increase toward unity.

F. Isochoric heat capacity

From (36) and (37) we know that the scaled internal energy $U/Nk_B T_v$ differs from the isochore (44) by a mere overall factor $\mathcal{D}/2$. The isochoric heat capacity, $C_v \doteq$

$\mathcal{N}^{-1}(\partial U/\partial T)_v$, derived from that expression reads

$$\frac{C_v}{k_B} = \frac{\mathcal{D}}{2} \left[\left(\frac{\mathcal{D}}{2} + 1 \right) \frac{G_{\mathcal{D}/2+1}(z, g)}{G_{\mathcal{D}/2}(z, g)} - \frac{\mathcal{D}}{2} \frac{G_{\mathcal{D}/2}(z, g)}{G_{\mathcal{D}/2-1}(z, g)} \right]. \quad (58)$$

In Fig. 7 we show plots of C_v/k_B versus T/T_v from (44) for various g and \mathcal{D} . In $\mathcal{D} = 2$ the heat capacity is independent of g , a result known since 1964 for the

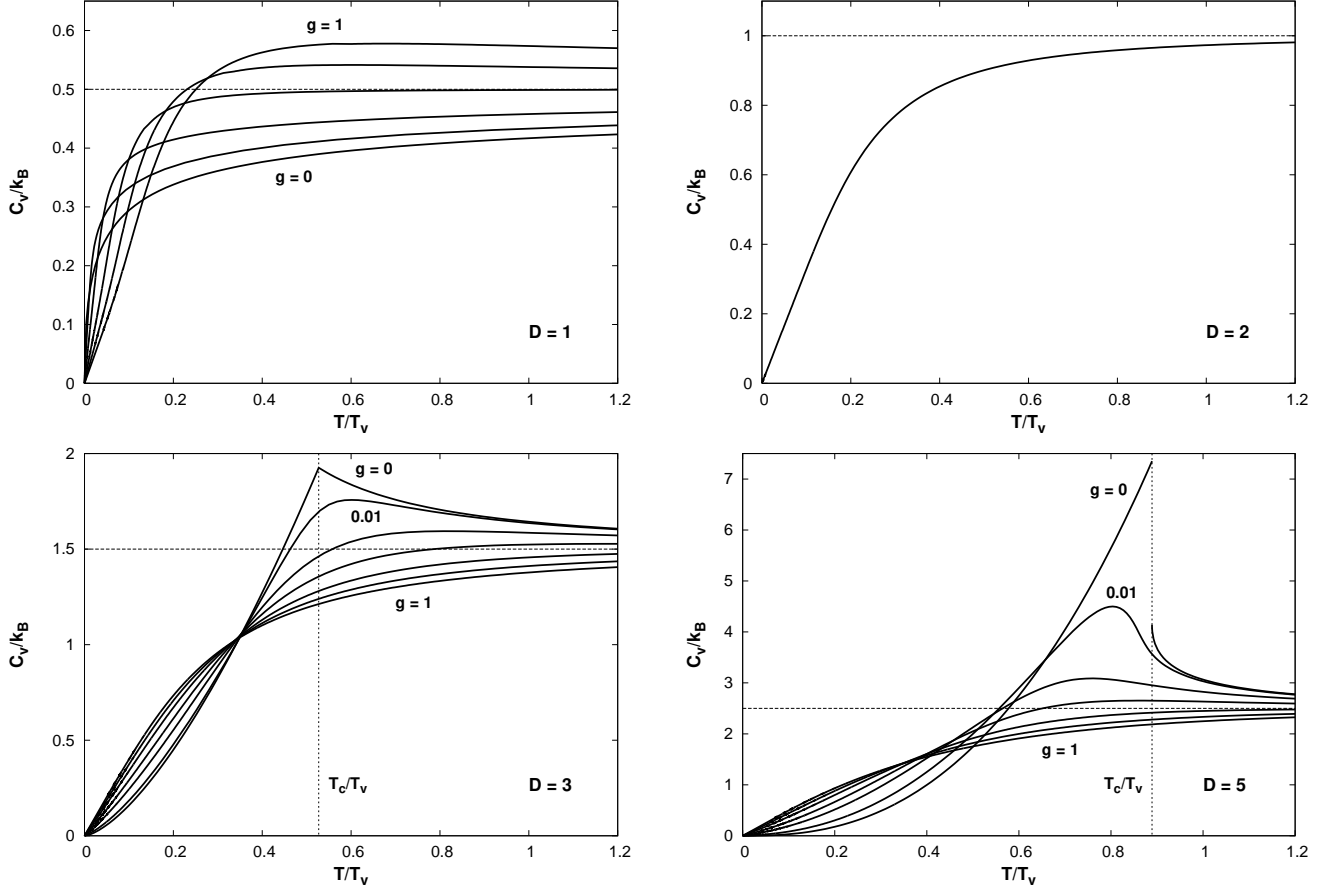


FIG. 7: Heat capacity in $\mathcal{D} = 1, 2, \dots, 5$ for $g = 0, 0.01, 0.1, 0.25, 0.5, 0.75, 1$ (from top down or bottom up). In $\mathcal{D} = 1$ the curves for $g = 0, 0.01$ are unresolved. In $\mathcal{D} = 2$ the heat capacity is independent of g . In $\mathcal{D} = 5$ the heat capacity has a discontinuity $\Delta C_v/k_B \simeq 3.21$ at T_c . Note the different vertical scales.

FD and BE gases and recently extended to $0 < g < 1$ [25, 26, 27, 28, 29]:

$$\frac{C_v}{k_B} = \frac{\pi^2}{3} \frac{T}{T_v} - \frac{T_v}{T} \sum_{n=1}^{\infty} \left(1 + \frac{2}{n} \frac{T}{T_v} + \frac{2}{n^2} \frac{T^2}{T_v^2} \right) e^{-nT_v/T} \quad (59)$$

In $\mathcal{D} < 2$ only the curves for $g > \frac{1}{2}$ have a local maximum and in $\mathcal{D} > 2$ only the curves for $g < \frac{1}{2}$. This double switch is reflected in the leading correction to the MB behavior at high T :

$$\frac{C_v}{k_B} \underset{T \rightarrow \infty}{\rightsquigarrow} \frac{\mathcal{D}}{2} \left[1 + \frac{(1/2 - g)(\mathcal{D}/2 - 1)}{2^{\mathcal{D}/2}} \left(\frac{T_v}{T} \right)^{\mathcal{D}/2} \right]. \quad (60)$$

The leading low- T behavior of C_v is linear for all $g > 0$:

$$\frac{C_v}{k_B} \underset{T \rightarrow 0}{\rightsquigarrow} \frac{\pi^2}{6} \frac{\mathcal{D} g^{(\mathcal{D}-2)/\mathcal{D}}}{[\Gamma(\mathcal{D}/2 + 1)]^{2/\mathcal{D}}} \frac{T}{T_v}. \quad (61)$$

In $\mathcal{D} < 2$ ($\mathcal{D} > 2$), the initial slope increases (decreases) with decreasing g , in agreement with the numerical results of Fig. 7.

The well-known power-law behavior of the bosonic heat capacity at low T reads

$$\frac{C_v}{k_B} \xrightarrow{T \rightarrow 0} \frac{\mathcal{D}}{2} \left(\frac{\mathcal{D}}{2} + 1 \right) \zeta \left(\frac{\mathcal{D}}{2} + 1 \right) \left(\frac{T}{T_c} \right)^{\mathcal{D}/2}. \quad (62)$$

It represents the leading singularity of the exact result in $\mathcal{D} \leq 2$ and, at the same time, the exact result itself for $0 \leq T \leq T_c$ in $\mathcal{D} > 2$. The latter result can be rewritten in the form

$$\frac{C_v}{k_B} = \frac{\mathcal{D}}{2} \left(\frac{\mathcal{D}}{2} + 1 \right) \frac{\zeta(\mathcal{D}/2 + 1)}{\zeta(\mathcal{D}/2)} \left(\frac{T}{T_c} \right)^{\mathcal{D}/2} \quad (63)$$

for $0 \leq T \leq T_c$ with T_c from (47).

Inspection of the bosonic heat capacity results (58) and (63) for $T \rightarrow T_c$ from above and below, respectively, in

$\mathcal{D} > 2$ shows a qualitative change of behavior in $\mathcal{D} = 4$. In $2 < \mathcal{D} \leq 4$ the heat capacity C_v has a local maximum at T_c with a discontinuous slope. In $\mathcal{D} > 4$ the function itself becomes discontinuous at T_c as is evident in Fig. 7. The size of the discontinuity is

$$\frac{\Delta C_v}{k_B} = \frac{\mathcal{D}^2}{4} \frac{\zeta(\mathcal{D}/2)}{\zeta(\mathcal{D}/2 - 1)} \quad (\mathcal{D} > 4). \quad (64)$$

There is no latent heat. Only in the limit $\mathcal{D} \rightarrow \infty$ a first-order transition emerges. In large \mathcal{D} the heat capacity stays very close to zero from $T = 0$ up to the near vicinity of T_c , where it shoots up to a high value of $O(\mathcal{D}^2)$. At T_c it drops back to a value of $O(\mathcal{D})$ and remains nearly constant. In the limit $\mathcal{D} \rightarrow \infty$ this spike turns into a delta function and its weight determines the latent heat.

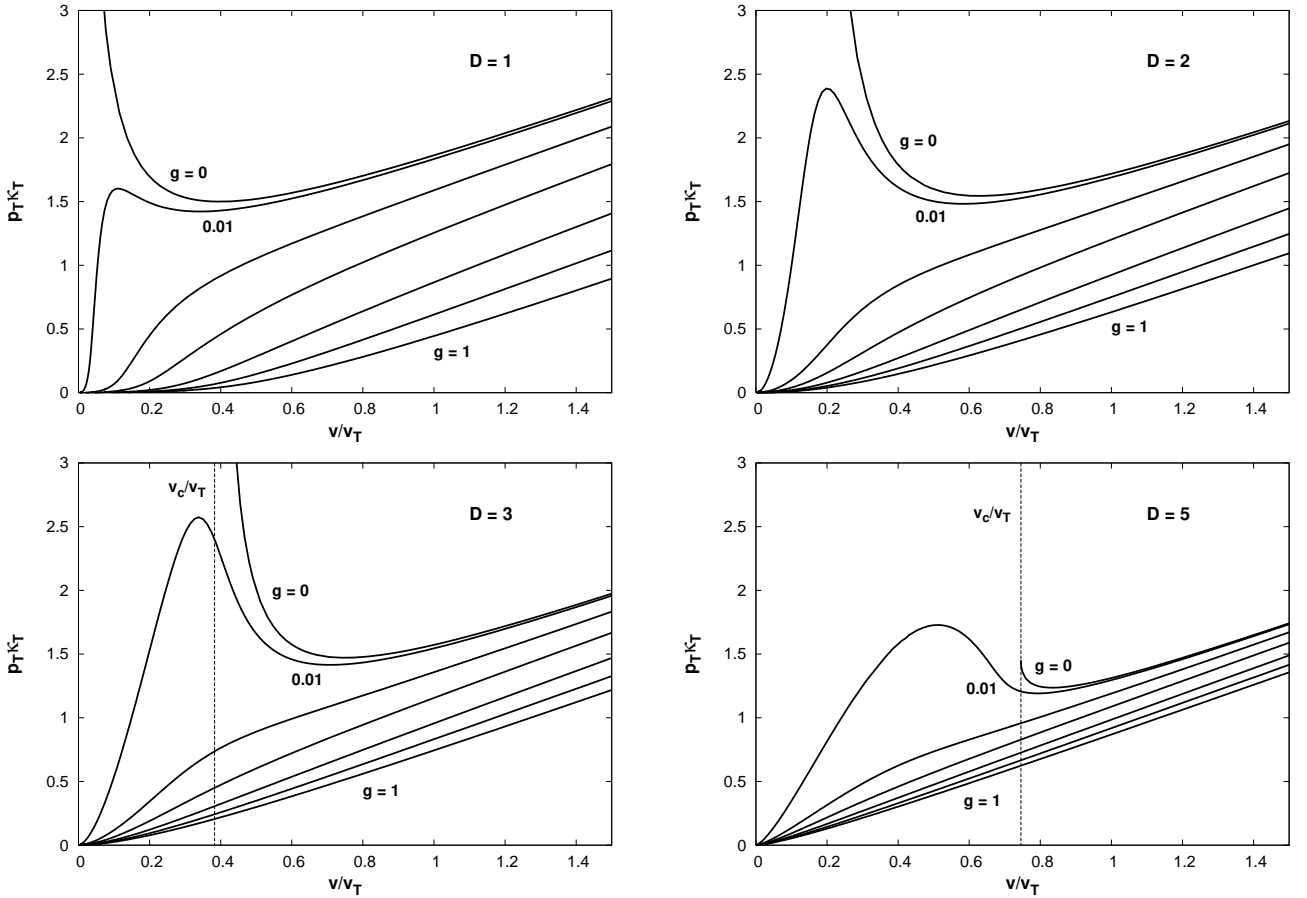


FIG. 8: Isothermal compressibility in $\mathcal{D} = 1, 2, 3, 5$ for $g = 0, 0.01, 0.1, 0.25, 0.5, 0.75, 1$ (from top down). The endpoint value of the bosonic curve in $\mathcal{D} = 5$ is $p_T \kappa_T \simeq 1.45$.

G. Isothermal compressibility

We obtain the following parametric representation of $\kappa_T \doteq -v^{-1}(\partial v / \partial p)_T$ from (49):

$$p_T \kappa_T = \frac{v}{v_T} \frac{G_{\mathcal{D}/2-1}(z, g)}{G_{\mathcal{D}/2}(z, g)}, \quad (65)$$

with v/v_T from (49). In Fig. 8 we plot $p_T \kappa_T$ versus v/v_T for various g and \mathcal{D} .

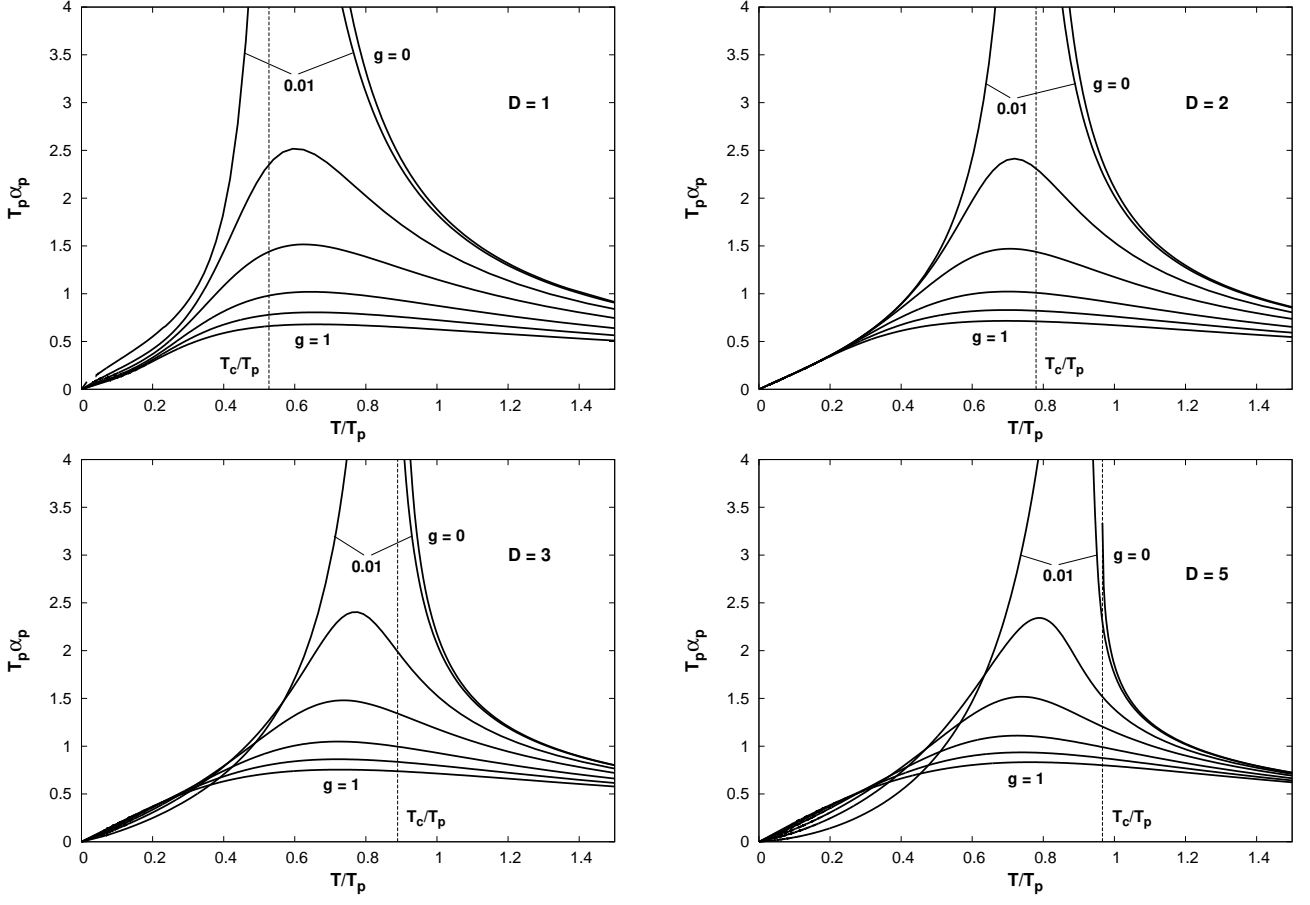


FIG. 9: Isobaric expansivity in $\mathcal{D} = 1, 2, 3, 5$ for $g = 0, 0.01, 0.1, 0.25, 0.5, 0.75, 1$ (from top down almost everywhere). The smooth maximum for $g = 0.01$ has the value $T_p \alpha_p \simeq 8.77, 9.69, 9.49, 6.84$ in $\mathcal{D} = 1, 2, 3, 5$, respectively. The endpoint value of the bosonic curve in $\mathcal{D} = 5$ is $T_p \alpha_p \simeq 3.34$.

The leading correction to MB behavior at low density, $v/v_T \gg 1$,

$$p_T \kappa_T \underset{v \rightarrow \infty}{\rightsquigarrow} \frac{v}{v_T} \left[1 + \frac{1/2 - g v_T}{2^{\mathcal{D}/2 - 1} v} \right], \quad (66)$$

is strongest in low \mathcal{D} . The compressibility curves for $g > \frac{1}{2}$ display fermion-like behavior across the entire range of v/v_T . The value of κ_T stays below the MB value and decreases monotonically with decreasing v/v_T , approaching zero in the limit $v \rightarrow 0$, reflecting the repulsive core of the statistical interaction. For $g < \frac{1}{2}$, by contrast, the curves start out above the MB line. Here the long-range attractive part of the statistical interaction is dominant, producing boson-like behavior. As the particle density increases a crossover from boson-like behavior at low density to fermion-like behavior at high density manifests itself as a shoulder or as a precipitous drop after a smooth local maximum. The leading high-density term of all compressibility curves for $g > 0$ is a

power-law with \mathcal{D} -dependent exponent:

$$p_T \kappa_T \underset{v \rightarrow 0}{\rightsquigarrow} \frac{\mathcal{D}}{2g^{2/\mathcal{D}} [\Gamma(\mathcal{D}/2 + 1)]^{2/\mathcal{D}}} \left(\frac{v}{v_T} \right)^{\frac{\mathcal{D}+2}{\mathcal{D}}}. \quad (67)$$

The uppermost curve in each panel of Fig. 8 is for bosons. It shares with all the other curves a decreasing initial trend as v/v_T is lowered in the low-density regime. Then it goes through a smooth minimum (a property shared with curves for $g \ll 1$) and rises to either a divergence or a cusp at v_c . In $\mathcal{D} \leq 2$ we have $v_c = 0$. Here the isothermal compressibility exhibits a power-law divergence, $\kappa_T \sim (v/v_T)^{-\mathcal{D}/(2-\mathcal{D})}$, in $1 \leq \mathcal{D} < 2$, and an exponential divergence, $\kappa_T \sim (v/v_T)^2 e^{v/v_T}$, in $\mathcal{D} = 2$. In $2 < \mathcal{D} \leq 4$ we have $v_c > 0$ as given in (53) and κ_T still diverges. However, in $\mathcal{D} > 4$ the divergence turns into a cusp at $p_{T_c} \kappa_{T_c} = \zeta(\mathcal{D}/2 - 1) / [\zeta(\mathcal{D}/2)]^2$. At $v < v_c$ we have $\kappa_T = \infty$.

H. Isobaric expansivity

We calculate $\alpha_p \doteq v^{-1}(\partial v/\partial T)_p$ from the general relation $\alpha_p = \kappa_T(\partial p/\partial T)_v$ and the CS-specific relation $C_v = (\mathcal{D}/2)v(\partial p/\partial T)_v$ to arrive at

$$T_p\alpha_p = \frac{T_p}{T} \left[\left(\frac{\mathcal{D}}{2} + 1 \right) \frac{G_{\mathcal{D}/2+1}(z, g)G_{\mathcal{D}/2-1}(z, g)}{G_{\mathcal{D}/2}(z, g)G_{\mathcal{D}/2}(z, g)} - \frac{\mathcal{D}}{2} \right] \quad (68)$$

with T/T_p from (54). In Fig. 9 we show expansivity curves $T_p\alpha_p$ versus T/T_p for various g and \mathcal{D} . We observe that the correction to MB behavior at high T is such that the expansivity is suppressed for $g > \frac{1}{2}$ and enhanced for $g < \frac{1}{2}$:

$$T_p\alpha_p \xrightarrow{T \rightarrow \infty} \frac{T_p}{T} \left[1 + \frac{(1/2 - g)(\mathcal{D}/2 + 1)}{2^{\mathcal{D}/2}} \left(\frac{T_p}{T} \right)^{\mathcal{D}/2+1} \right]. \quad (69)$$

The characteristic features of all compressibility curves for $0 < g < 1$ are a smooth maximum and a linear approach to zero in the low- T limit. The maximum is flat near the fermion limit and becomes increasingly high and narrow as the boson limit is approached. For $g \ll 1$ the position of the maximum is close to the bosonic T_c as given in (57). The slope of the linear low- T behavior of α_p depends on g and \mathcal{D} :

$$T_p\alpha_p \xrightarrow{T \rightarrow 0} \frac{\pi^2}{6} \frac{\mathcal{D}g^{(\mathcal{D}-2)/(\mathcal{D}+2)}}{[\Gamma(\mathcal{D}/2 + 1)]^{4/(\mathcal{D}+2)}} \frac{T}{T_p}. \quad (70)$$

Note the absence of any g -dependence in $\mathcal{D} = 2$ and the opposite trends regarding g -dependence in $\mathcal{D} < 2$ and $\mathcal{D} > 2$ reminiscent of trends seen in the heat capacity.

The bosonic expansivity increases monotonically with decreasing T and ends in a singularity as T_c is approached from above. In $\mathcal{D} \leq 4$ the singularity is a divergence and in $\mathcal{D} > 4$ it is a cusp.

I. Velocity of sound

We start from the relation $c = (\rho\kappa_S)^{-1/2}$ for the velocity of sound, where $\rho = m/v$ is the mass density and κ_S the adiabatic compressibility. We use standard relations between response functions to arrive at the following expression, all in terms of dimensionless entities previously determined [30]:

$$\frac{mc^2}{k_B T} = \frac{(v/v_T)}{(p_T\kappa_T)} \left[1 + \frac{(T/T_p)^2(v/v_T)(T_p\alpha_p)^2}{(p_T\kappa_T)(C_v/k_B)} \right]. \quad (71)$$

For the CS model the right-hand side of (71) can be greatly simplified:

$$\frac{mc^2}{k_B T} = \gamma \frac{G_{\mathcal{D}/2+1}(z, g)}{G_{\mathcal{D}/2}(z, g)}, \quad \gamma \doteq 1 + \frac{2}{\mathcal{D}}. \quad (72)$$

How does the velocity of sound c vary with temperature T if we keep the (average) particle density $1/v$ or the (average) pressure p fixed? Remarkably, we find very simple universal relations between c and the isochore or isobar itself for the two situations, respectively:

$$\frac{mc^2}{k_B T_v} = \gamma \frac{p}{p_v} \quad (v = \text{const.}), \quad (73)$$

$$\frac{mc^2}{k_B T_p} = \gamma \frac{v}{v_p} \quad (p = \text{const.}), \quad (74)$$

with the dependence of p/p_v on T/T_v as discussed in Sec. IV C and the dependence of v/v_p on T/T_p as discussed in Sec. IV E.

We conclude that c has a monotonic dependence on T no matter whether we keep v or p constant. for $g > 0$ the velocity of sound stays nonzero in the limit $T \rightarrow 0$. In the boson gas c is affected by the onset of BEC. There are no sound waves in the condensate. The isochores at $T < T_c$ in Fig. 4 or the vertical portions of the isobars at $T = T_c$ in Fig. 6 give us information about c in the gas coexisting with the condensate.

V. EFFECTS OF SOFT TRAP WALLS

Consider an ideal quantum gas in $\mathcal{D} \geq 1$, trapped by a spatially isotropic power-law potential [7, 8]

$$\mathcal{U}(r) \doteq \mathcal{U}_0 \left(\frac{r}{R} \right)^\eta, \quad (75)$$

where r is the radial coordinate in \mathcal{D} -dimensional space. The size of the trap is determined by the ‘‘width’’ R and the ‘‘depth’’ \mathcal{U}_0 of the potential well. The softness of the confinement is controlled by the exponent η . Harmonic traps have $\eta = 2$. Lowering the value of η makes the surrounding wall softer, increasing it makes the wall harder. For $\eta \rightarrow \infty$, the wall becomes rigid and the bottom of the potential becomes flat, which corresponds to the situation considered in Sec. IV.

Softening the trap walls affects the density of energy levels. For the power-law potential (75) expression (28) must be replaced by

$$D(\epsilon_0) = \frac{\mathcal{V}}{2^{\mathcal{D}}\pi^{\mathcal{D}/2}\Gamma(\mathcal{D}/2)} \epsilon_0^{\mathcal{D}/2-1} \left(\frac{\epsilon_0}{\mathcal{U}_0} \right)^{\mathcal{D}/\eta} Q_{\mathcal{D}}(\eta) \quad (76)$$

with

$$\mathcal{V} = \frac{\pi^{\mathcal{D}/2}}{\Gamma(\mathcal{D}/2 + 1)} R^{\mathcal{D}}, \quad Q_{\mathcal{D}}(\eta) \doteq \frac{\Gamma(\mathcal{D}/\eta + 1)\Gamma(\mathcal{D}/2)}{\Gamma(\mathcal{D}/\eta + \mathcal{D}/2)}. \quad (77)$$

In soft-wall traps it makes sense to consider processes at $\mathcal{V} = \text{const}$ instead of isochoric processes. Under these circumstances the gas expands when heated up. In generalization of relations (36) and (37) we now have

$$\mathcal{N} = \frac{\mathcal{V}}{\lambda_T^{\mathcal{D}}}\Gamma(\mathcal{D}/\eta + 1) \left(\frac{k_B}{\mathcal{U}_0} \right)^{\mathcal{D}/\eta} G_{\mathcal{D}/2+\mathcal{D}/\eta}(z, g), \quad (78)$$

$$U = \frac{\mathcal{V}k_B T}{\lambda_T^{\mathcal{D}}} \left(\frac{k_B T}{\mathcal{U}_0} \right)^{\mathcal{D}/\eta} \times \Gamma \left(\frac{\mathcal{D}}{\eta} + 1 \right) \left(\frac{\mathcal{D}}{\eta} + \frac{\mathcal{D}}{2} \right) G_{\mathcal{D}/2+\mathcal{D}/\eta+1}(z, g). \quad (79)$$

As before, an additive term $z/(1-z)$ has to be considered in (78) if $g = 0$. We now use the reference temperature

$$T_v = \left(\frac{\mathcal{N}}{\mathcal{V}} \right)^{\frac{1}{\mathcal{D}/\eta+\mathcal{D}/2}} \left(\frac{4\pi}{k_B} \right)^{\frac{\mathcal{D}/2}{\mathcal{D}/\eta+\mathcal{D}/2}} \left(\frac{\mathcal{U}_0}{k_B} \right)^{\frac{\mathcal{D}/\eta}{\mathcal{D}/\eta+\mathcal{D}/2}} \times [\Gamma(\mathcal{D}/\eta + 1)]^{\frac{-1}{\mathcal{D}/\eta+\mathcal{D}/2}}. \quad (80)$$

For bosons the onset of BEC occurs at $T_c > 0$ in $\mathcal{D} > \mathcal{D}_m = 2\eta/(2 + \eta)$. The marginal dimensionality decreases from $\mathcal{D}_m = 2$ to $\mathcal{D}_m = 1$ as the rigid-wall container softens into a harmonic trap. The transition temperature in units of T_v is

$$\frac{T_c}{T_v} = [\zeta(\mathcal{D}/\eta + \mathcal{D}/2)]^{\frac{-1}{\mathcal{D}/\eta+\mathcal{D}/2}}. \quad (81)$$

VI. CONCLUSION AND OUTLOOK

We have explored the thermodynamics of the generalized CS model in $\mathcal{D} \geq 1$ dimensions. In this model the statistical interaction is limited to pairs of particles with identical momenta. This reduces the coupling, effectively, to a statistical exclusion condition. Several observed phenomena suggest the presence of a long-range attractive part and a short-range repulsive part in this particular statistical interaction.

The generalized CS model is found to preserve several attributes that are characteristic of the familiar ideal BE

and FD gases – attributes which may very well count as hallmarks of ideal quantum gases in general: (i) The average level occupancy $\langle n(\epsilon_0) \rangle$ is a unique function of $(\epsilon_0 - \mu)/k_B T$ for given g , independent of \mathcal{D} . (ii) The fundamental thermodynamic relations (35)–(37) for given g and with the prescribed structure on the left-hand side are unique functions of the fugacity z . (iii) The right-hand sides of Eqs. (35) and (37) are identical.

The consequences include that the isochore and the (properly scaled) internal energy have the same dependence on T , that the quantity $pV/\mathcal{N}k_B T$ has a unique dependence on z for given \mathcal{D} and that the square of the (properly scaled) velocity of sound at constant v (constant p) has the same T -dependence as the isochore (isobar). The thermodynamics of the generalized CS model as described in Sec. IV is thus ideally suited in the role of benchmark for the thermodynamics of gases with more generic statistical or dynamical interactions. From work in progress on several model systems in \mathcal{D} dimensions with statistical interactions not restricted as in (19), we have compelling evidence that none of the ideal quantum gas hallmarks (i)–(iii) are upheld anymore. The stage is thus set for the exact analysis of qualitatively new thermodynamic phenomena including phase transitions in non-bosonic quantum gases.

Acknowledgments

Financial support from the DFG Schwerpunkt *Kollektive Quantenzustände in elektronischen 1D Übergangsmetallverbindungen* (for M.K.) is gratefully acknowledged. G.M. is grateful to Prof. Dr. H. Thomas for stimulating discussions.

-
- [1] C. J. Pethick and H. Smith, *Bose-Einstein condensation in dilute gases* (Cambridge University Press, 2002).
 - [2] L. Pitaevskii and S. Stringari, *Bose-Einstein condensation* (Oxford University Press, 2003).
 - [3] M. Greiner, I. Bloch, O. Mandel, T. W. Hänsch et al., *Phys. Rev. Lett.* **87**, 160405 (2001).
 - [4] A. Görlitz, J. M. Vogel, A. E. Leanhardt, C. Raman et al., *Phys. Rev. Lett.* **87**, 130402 (2001).
 - [5] F. Schreck, L. Khaykovich, K. Corwin, G. Ferrari et al., *Phys. Rev. Lett.* **87**, 080403 (2001).
 - [6] D. S. Petrov, D. M. Gangardt, and G. V. Shlyapnikov, *J. Phys. IV France* **116**, 5 (2004).
 - [7] V. Bagnato, D. E. Pritchard, and D. Kleppner, *Phys. Rev. A* **35**, 4354 (1987).
 - [8] V. Bagnato and D. Kleppner, *Phys. Rev. A* **44**, 7439 (1991).
 - [9] F. D. M. Haldane, *Phys. Rev. Lett.* **67**, 937 (1991).
 - [10] Y. S. Wu, *Phys. Rev. Lett.* **73**, 922 (1994).
 - [11] D. Bernard and Y. S. Wu, in *New developments on integrable systems and long-ranged interaction models* (M. L. Ge and Y.-S. Wu eds.) (World Scientific, Singapore, 1994).
 - [12] B. Sutherland, *Beautiful models: 70 years of exactly solved quantum many-body problems* (World Scientific, Singapore, 2004).
 - [13] B. Sutherland, *J. Math. Phys.* **12**, 251 (1971).
 - [14] C. Nayak and F. Wilczek, *Phys. Rev. Lett.* **73**, 2740 (1994).
 - [15] S. B. Isakov, D. P. Arovas, J. Myrheim, and A. P. Polychronakos, *Phys. Lett. A* **212**, 299 (1996).
 - [16] G. S. Joyce, S. Sarkar, J. Spalek, and K. Byczuk, *Phys. Rev. B* **53**, 990 (1996).
 - [17] G. B. Potter, G. Müller, and M. Karbach, (unpublished).
 - [18] S. B. Isakov, *Int. J. Mod. Phys.* **9**, 2563 (1994).
 - [19] F. Calogero, *J. Math. Phys.* **12**, 419 (1971).
 - [20] B. Sutherland, *Phys. Rev. A* **4**, 2019 (1971).
 - [21] B. Sutherland, *Phys. Rev. A* **5**, 1372 (1972).
 - [22] C. N. Yang and C. P. Yang, *J. Math. Phys.* **10**, 1115 (1969).
 - [23] E. Lieb and W. Liniger, *Phys. Rev.* **130**, 1605 (1963).
 - [24] M. V. N. Murthy and R. Shankar, *Phys. Rev. B* **60**, 6517 (1999).

- [25] R. M. May, Phys. Rev. **135**, A1515 (1964).
- [26] S. Viefers, F. Ravndal, and T. Haugset, Am. J. Phys. **63**, 369 (1995).
- [27] M. H. Lee, Phys. Rev. E **55**, 1518 (1997).
- [28] A. Swarup and B. Cowan, J. Low Temp. Phys. **134**, 881 (2004).
- [29] D.-V. Anghel, J. Phys. A **35**, 7255 (2002).
- [30] For consistency, we must use reference values T_p , T_v , v_T derived from the first expression (38) of λ_T in this context.